Journal of Catalysis 262 (2009) 314–323

Contents lists available at ScienceDirect

Journal of Catalysis

www.elsevier.com/locate/jcat

Bimetallic PdAu–KOac/SiO_2 catalysts for vinyl acetate monomer (VAM) synthesis: Insights into deactivation under industrial conditions

Marga-Martina Pohl [a,*], Jörg Radnik [a], Matthias Schneider [a], Ursula Bentrup [a], David Linke [a], Angelika Brückner [a], Ewen Ferguson [b]

[a] Leibniz-Institute for Catalysis e.V. (Branch Berlin), Richard-Willstätter-Str. 12, D-12489 Berlin, Germany
[b] BP Chemicals Ltd, Saltend, Hull, HU12 8DS, UK

ARTICLE INFO

Article history:
Received 14 November 2008
Revised 15 January 2009
Accepted 15 January 2009
Available online 31 January 2009

Keywords:
Alloy
Silica supported palladium gold catalysts
Deactivation
TEM/EDXS
XRD
XPS
FTIR

ABSTRACT

Structural changes of a commercial supported PdAu/SiO_2 catalyst for VAM production aged under laboratory and industrial conditions were studied by XRD, TEM/EDXS, XPS, ICP-OES and FTIR spectroscopy. The fresh catalyst contains alloy particles with a wide range of Pd/Au ratios formed by agglomerated crystallites of different sizes. The particles do not show any noticeable sintering during deactivation up to 6 month use but undergo serious restructuring which is connected to the migration of Pd to the particle surface during early stages on stream followed by formation of water-soluble Pd, most probably Pd acetate, which is leached out of the catalyst upon extended time on stream. Considering earlier studies which identified single Pd atoms isolated from each other by surrounding Au atoms as active sites [M. Chen, D. Kumar, C.-W. Yi, D.W. Goodman, Science 310 (2005) 291], it is concluded that the partial enrichment of Pd on the exposed noble metal alloy surface is a major reason for loss of activity in the present type of catalyst. Additionally it is demonstrated that simultaneous calculation of crystallite sizes and alloy compositions from the width and position of the XRD reflections, as usually performed, can in principal, give information on dynamic changes in the noble metal phase but it is not a meaningful approach for calculations both of crystallite size and composition in such inhomogeneous systems.

1. Introduction

Vinyl acetate monomer (VAM) with an annual production of about 3.5 million tons is an important commodity used for the synthesis of polyvinyl alcohol and polyvinyl acetate which in turn are used on a large scale for the production of fibres and coatings. Nowadays, VAM is mostly produced via gas-phase acetoxylation of ethylene over bimetallic supported Pd/Au catalysts which are additionally modified with potassium acetate (KOac) (Eq. (1)) [1].

$$C_2H_4 + CH_3COOH + 0.5O_2 \rightarrow CH_2CHC(O)OCH_3. \quad (1)$$

The role of the different catalyst components and, in particular, the oxidation state of active Pd species is still controversially discussed. Nakamura and Yasui consider a Pd(I)-acetate species formed by dissociative adsorption of acetic acid as active site. Reaction with a vinyl–Pd intermediate formed by dehydrogenation of ethylene leads to VAM in the rate determining step [2], while Pd(II) acetate was thought to be detrimental for both selectivity and activity since it favoured the formation of acetic aldehyde and the agglomeration of palladium [3]. In contrast, other authors related catalytic activity to a Pd(II) acetate species formed by oxidation of Pd(0) in the presence of acetic acid. Reaction of this intermediate with ethylene was supposed to lead to VAM and regeneration of acetic acid and Pd(0) [4]. This mechanism requires the presence of a condensed film of acetic acid and water on the catalyst surface, in which the reaction proceeds in a similar way as assumed for the homogeneously catalysed process [5]. The role of KOac was discussed to be retention of acetic acid within this liquid surface layer [5], promotion of a PdOac surface intermediate and weakening of the Pd–O bond within this intermediate to facilitate insertion of ethylene [1]. Very little is known about the role of Au though it was found that the presence of Au enhances VAM formation and suppresses combustion of acetic acid [6]. Based on studies of model Au(100) surfaces containing Pd pairs with optimised distances (0.33 nm), Goodman et al. proposed that the role of Au might be the spatial separation of Pd atoms, fixing them just at an optimum distance for high catalytic performance [7–9].

A serious problem for commercial PdAu/SiO_2 catalysts is deactivation which limits their useful lifetime within the reactor to a few years. Deactivation has a negative economic and environmental impact since it leads to lower VAM yields, poorer utilisation of raw materials and requires more frequent replacement of the

* Corresponding author.
E-mail address: marga-martina.pohl@catalysis.de (M.-M. Pohl).

0021-9517/$ – see front matter
doi:10.1016/j.jcat.2009.01.008

catalyst. Thus, a better understanding of the reasons for deactivation as a basis for improving the catalyst stability is of high industrial interest. Against this background, it is surprising that only very few studies on deactivation of VAM catalysts have been published so far [10–13]. Sintering of metal particles has been discussed as the main reason for irreversible catalyst deactivation. Some authors claim that sintering is connected to the formation of mobile Pd acetate species [3,11] while this has been excluded by others [13]. Besides sintering, diffusion of Au from the surface of the metal particles into the bulk and decomposition of the KOac promoter have also been discussed as reasons for irreversible deactivation [12]. The loss of KOac itself is not a technical problem since small amounts of this component are added to the feed of industrial reactors to compensate for the continuous loss of KOac during the reaction. In addition, adsorption of products and deposits, especially at low reaction temperature, was found to contribute to reversible deactivation [10,12].

There have been indications that the composition of the XRD-visible crystalline Pd/Au phase contains less Pd than expected from the total Pd/Au ratio in the catalyst, suggesting the presence of a Pd-rich XRD-invisible phase, the role of which was however not further discussed [13]. The composition of the crystalline Pd/Au phase was obtained from the peak positions using Vegard's rule while the metal particle size was derived from the peak width, disregarding the fact that the latter provides information only on the mean crystallite size while particles may consist of several agglomerated crystallites of different size and/or composition. Due to this ambiguity the results in [13] have to be considered with care.

It is the aim of this work to elucidate changes of supported Pd/Au catalysts caused by different times on stream as a basis for identifying reasons for deactivation. With respect to the above mentioned contradictory opinions on the role of mobile Pd species as well as ambiguities resulting from XRD studies, a variety of different characterisation methods was used to gain comprehensive information on structure, composition and morphology of the metal crystallites and particles as well as on the composition of the metal alloy phase and their changes related to deactivation phenomena.

2. Experimental

2.1. Catalysts

The catalysts used were KOac promoted $PdAu/SiO_2$ catalysts in fresh form (sample F) as well as a six month old used sample (sample 6m). Additionally, the fresh catalyst F was aged for 70 h in a laboratory fixed bed reactor using the standard protocol described below (sample 70h). To derive information on possible soluble Pd species, the three catalysts were not only studied in as-received form but also after removal of KOac by washing with water. The KOac-free samples are designated as F-K, 6m-K and 70h-K.

2.2. Removal of potassium acetate

2 g of catalyst was subsequently washed with four portions of 50 ml deionised water in a porosity 3 filter funnel by stirring the suspension with a PTFE spatula for about 30 min. After settling, water was pumped off. The catalyst was transferred into an evaporation dish and dried at 120 °C overnight.

2.3. Laboratory ageing procedure

After pressurising the catalyst with 9 bar N_2 and heating to 150 °C, the reactants (C_2H_4:AcOH:O_2:N_2 = 70:10:5:15; GHSV = 8000 h^{-1} STP) were added to the N_2 stream within 30 min following the sequence: (1) ethylene, (2) acetic acid and (3) O_2. After 20 h, the oxygen concentration was raised to 7% and maintained for another 50 h. During this treatment, the catalyst lost about 20% of its initial activity and reached a steady state in which selectivity became stable and deactivation was markedly slower.

2.4. XRD measurements

All samples were measured at room temperature with Cu$K_{\alpha 1}$ radiation in the 2θ range of 25° to 90° (in steps of 0.25° with 150 s per step) using a STADI P automated transmission diffractometer (Stoe, Darmstadt, Germany) equipped with a linear PSD. For the exact determination of peak position and quantification of the percentage of crystalline Pd/Au alloy, an internal crystalline NIST standard (5% Si) was used. An external LaB_6 NIST standard with sharp peaks was used to determine the instrumental resolution function. Pattern fitting (pseudo-Voigt function, Chebyshev polynomial as background function, peak asymmetry correction) was carried out with the Win X^{POW} program package, using the Powder Diffraction Files (PDF) of the International Centre of Diffraction Data (ICDD). The cubic lattice constant of the Pd/Au alloy phase was derived from the exact positions of all observable alloy peaks. With these values, the alloy composition was determined using Vegard's rule. The mean metal crystallite size was obtained from the full width at half maximum (FWHM) of the XRD peaks using the Scherrer equation. Quantitative calculations of the amount of crystalline phase were performed as Rietveld refinement with the program POWDER CELL.

2.5. TEM/EDXS measurements

TEM micrographs were recorded with a CM20 microscope (FEI) equipped with a STwin and LaB_6, at 200 kV. For EDX measurements without internal standard a PV9900 analyser (EDAX) was used with spot sizes of approximately 35 nm. For quantitative measurements, only spectra with less than 10% error for the gold L and gold M lines were used. The samples were prepared by depositing the catalyst after grinding on copper grids (mesh 300) covered by Lacey carbon.

2.6. XPS measurements

X-ray photoelectron spectra were recorded on a VG ESCALAB 220iXL with MgK_α radiation (E = 1253.6 eV). The samples were fixed by a double-sided adhesive carbon tape on the stainless steel sample holder. The electron binding energy was referenced to the C 1s peak at 284.8 eV. The peaks were fitted by Gaussian–Lorentzian profiles after a Shirley background subtraction. For quantitative analysis, the peak area was divided by the element-specific Scofield factors and the transmission function of the analyser. The residual pressure in the chamber was lower than 10^{-7} Pa.

2.7. ICP-OES analysis

5 mg catalyst was dissolved in 3 ml aqua-regia and 5 ml HF in a microwave oven (CEM MDS-2000) at 4 bar. The obtained solution was filled up to 100 ml with distilled water. ICP measurements were performed with a Perkin Elmer ICP-OES Optima 3000XL spectrometer calibrated for the required elements. All values were verified by double determination.

2.8. FTIR measurements

All studies were performed with KOac free samples. The spectra were recorded using a Bruker IFS 66 spectrometer equipped with

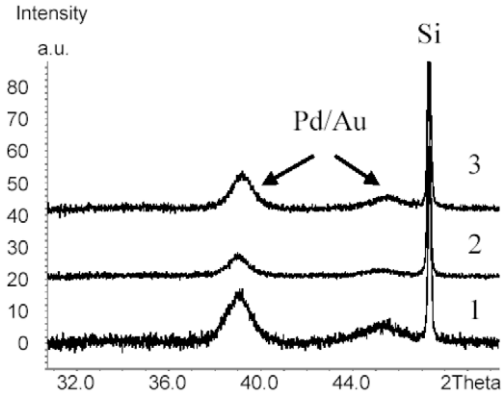

Fig. 1. Experimental background-corrected XRD powder patterns of samples F (1), 70h (2) and 6m (3) measured with silicon standard. Intensity range is chosen for proper display of alloy peaks.

Table 1
Mean crystallite size, cubic lattice constant, alloy composition and percentage of crystalline alloy phase derived from XRD powder patterns.

Sample	Mean crystallite size (nm)	Lattice constant (Å)	Alloy composition	Percentage of crystalline alloy (%)
F	3.8	3.996	$Au_{1.1}Pd_{0.9}$	55.4
70h	4.1	3.998	$Au_{1.1}Pd_{0.9}$	8.2
6m	5.0	3.980	Au_1Pd_1	30.0

a heatable and evacuable IR cell with CaF_2 windows, connected to a gas dosing–evacuating system. For CO adsorption measurements, the ground catalyst powder was pressed into self-supporting discs (50 mg, diameter 20 mm) and activated by heating to 200 °C under vacuum for 1 h followed by cooling to room temperature. CO was adsorbed at room temperature until saturation using a 5% CO/He mixture. Spectra were recorded after evacuation at room temperature with a resolution of 2 cm^{-1} and 100 scans. Background-corrected spectra were obtained by subtraction of the spectrum of the activated sample at room temperature from the adsorbate spectrum, respectively.

3. Results

3.1. XRD results

XRD measurements were performed with as-received KOac-containing samples for deriving the percentage of the crystalline Pd/Au phase, the Pd/Au alloy composition as well as the mean Pd/Au crystallite size using the procedures described in the experimental part. The powder patterns of all samples show, as expected, identical intensities and positions for the silicon peak at 47.5° but differences in intensity and less pronounced, also in the peak position for the Pd/Au alloy peaks at 39.0° and 45.5°. This suggests that the mean crystallite size in the three catalysts differs more than the Pd/Au alloy composition (Fig. 1). Lattice constants and Pd/Au alloy compositions, obtained by fitting all four observable Pd/Au peaks at 39.0°, 45.3°, 66.0° and 78.9°, are listed in Table 1. For the single components and for a 1:1 alloy the following cubic lattice constants are available from data bases (ICSD, ICDD): Au ($a = 4.080$ Å), Pd ($a = 3.890$ Å), Au_1Pd_1 ($a = 3.980$ Å). By comparing these values with those in Table 1, it is obvious that the Pd/Au alloy ratio in the catalysts is very close to unity. This is much lower than expected, when considering the total Pd/Au ratio derived from chemical analysis which is 4.6. It suggests that there might be a considerable percentage of Pd which is not accessible by XRD.

Table 1 also shows that only about half of the total alloy amount in sample F is crystalline. In sample 70h the crystalline alloy percentage even dropped to 8.2% while it increases again to 30.0% in sample 6m. This suggests that a considerable percentage of the crystalline Pd/Au alloy present in the fresh catalyst F might become amorphous during equilibration and recrystallises again partly during 6 month use.

Since the observed Pd/Au peaks are in all cases very broad with FWHM values between 1.2° and 2.9°, calculated mean crystallite sizes do not exceed 5 nm (Table 1). The mean crystallite size for both used samples 70h and 6m is higher than for the fresh sample F. Together with the values for the crystalline percentage, this suggests that a certain part of the alloy becomes amorphous while the crystallites of the remaining part grow.

3.2. TEM/EDXS results

By HRTEM changes of the crystallite size of the noble metals were analysed and the edges of these single crystallites were investigated for the appearance of amorphous layers which could explain the low percentage of crystalline material in the alloy. The differences in the lattices of Pd and Au and all of their mixtures are too small to derive reliable information on the crystallite composition by measuring the lattice planes in the images. Thus, inhomogeneity could only be detected by performing quantitative EDX measurements on single particles or small particle agglomerates (about 35 nm spots), which usually consist of several single crystallites. 50 different areas of each sample were analysed and the compositional distributions were calculated.

Typical images of the morphology are shown in Fig. 2 before and in Fig. 3 after KOac removal. In all samples, small particles as well as agglomerates bigger than 100 nm located on the silica support particles are observed. Due to the anisotropic shape, the overlap of particles and large differences in size, a statistical evaluation for calculating particle size distributions is not meaningful. A variety of Pd/Au ratios was found for small spots from different particle agglomerates by EDXS which, in contrast to XRD results (Table 1), show an excess of Pd in all cases (inserts in Figs. 2 and 3). Typical high-resolution snapshots clearly show the presence of crystallites of up to more than 10 nm size, which is much bigger than derived from XRD powder patterns (Fig. 4, Table 1). This illustrates the limitations of XRD for deriving such data on mean composition and crystallite size when studying such inhomogeneous samples. This will be discussed in more detail below.

To get more information on changes of the composition of the noble metal phase upon ageing, a series of EDXS measurements of agglomerates of some crystallites within a 35 nm spot was performed. Therefore, these EDXS measurements do not provide information on single crystallites. Fig. 5 shows the Pd/Au ratio distributions of the samples before (black columns) and after removal of potassium acetate (grey columns). In all cases no particles with gold excess were found but several particles with very high Pd content up to pure Pd. In all samples, the majority of EDXS measurements reflects noble metal areas with almost the theoretical Pd/Au ratio which is 4.6. During the first 70 h on stream (sample 70h), the distribution is virtually not changed, apart from the fact that slightly more particle areas with very high Pd content were detected. After 6 month use (sample 6m) a narrower and pronounced maximum around the theoretical Pd/Au ratio and a pronounced Pd rich tail is detected.

The influence of KOac removal is particularly evident for the most deactivated sample 6m-K from the grey columns in Fig. 5. Almost no change of the distribution around the maximum at the theoretical Pd/Au ratio is found after KOac removal for the fresh sample F-K and only minor changes occur for sample 70h-K. In contrast, the narrow maximum reflecting particle areas with al-

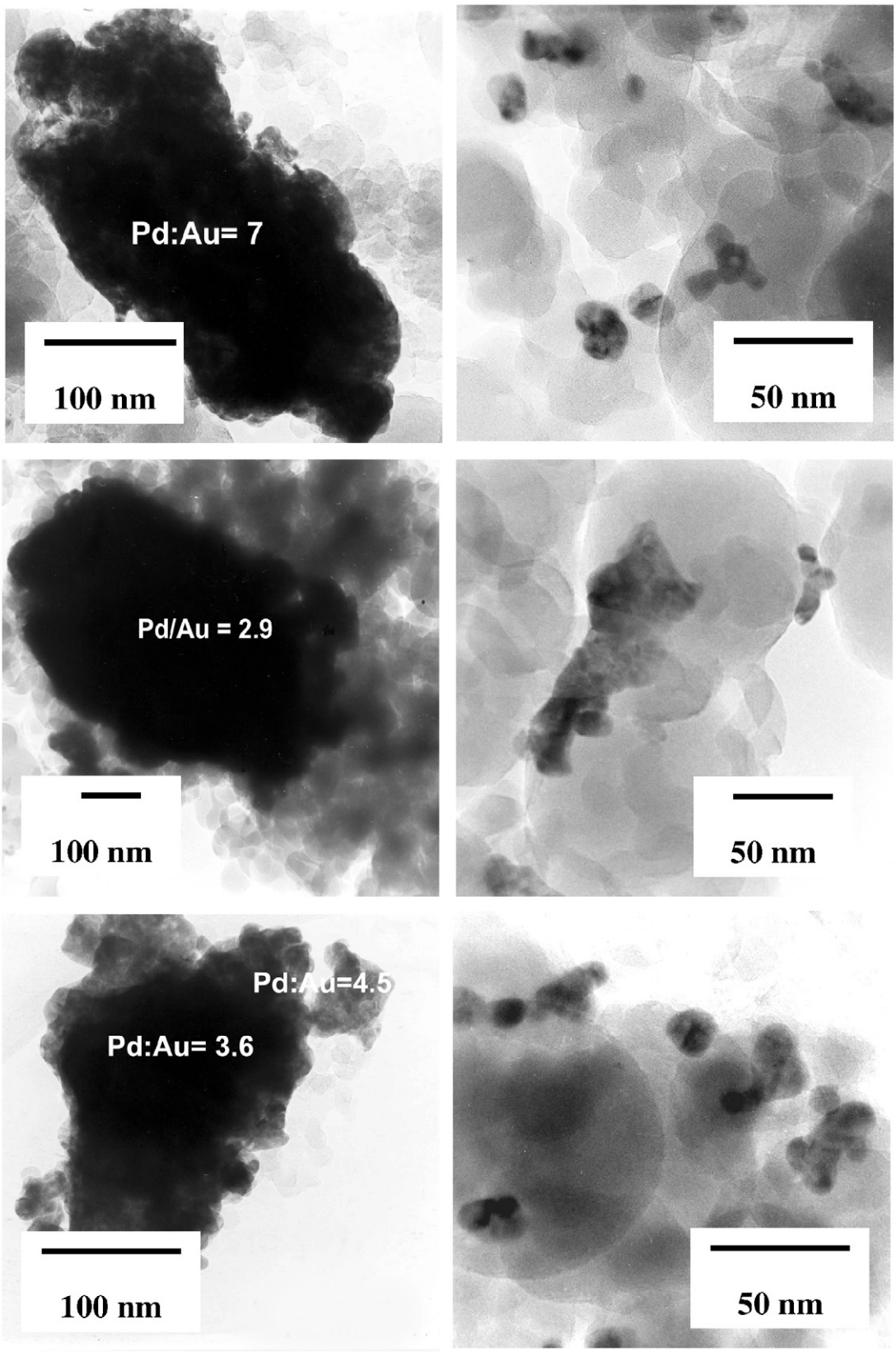

Fig. 2. TEM images showing metal particles of different size in samples F (top), 70h (middle) and 6m (bottom) together with Pd/Au ratios determined by EDX from an arbitrarily chosen 30 nm spot within a metal particle.

most the theoretical Pd/Au in sample 6m is weakened after KOac removal (sample 6m-K, Fig. 5). For both aged samples the number of particles with very high Pd content is increased. This suggests that some kind of mobile Pd species may have formed during 6 months use which can be redistributed by the water treatment procedure applied for KOac removal.

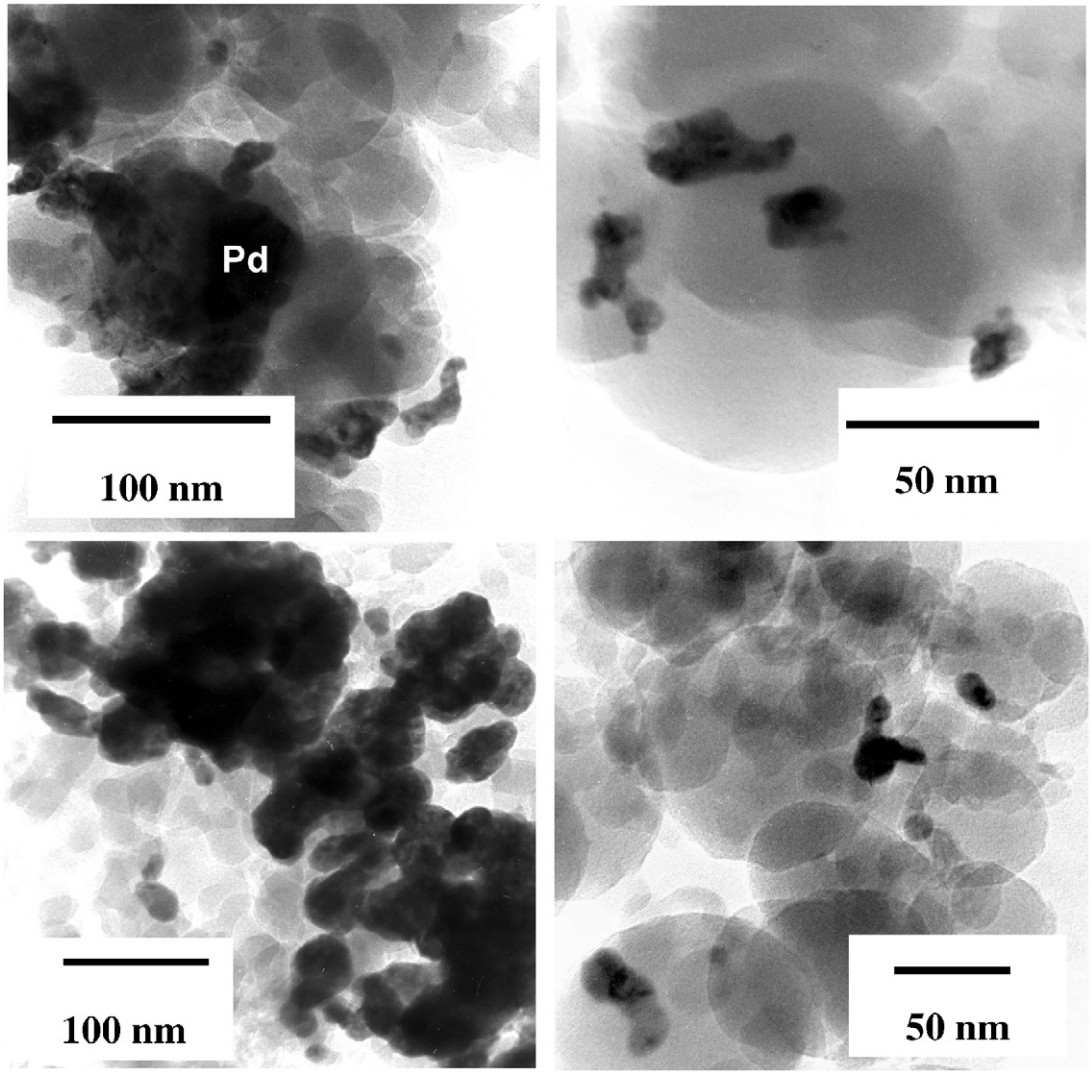

Fig. 3. TEM images showing metal particles of different size in samples 70h-K (top) and 6m-K (bottom).

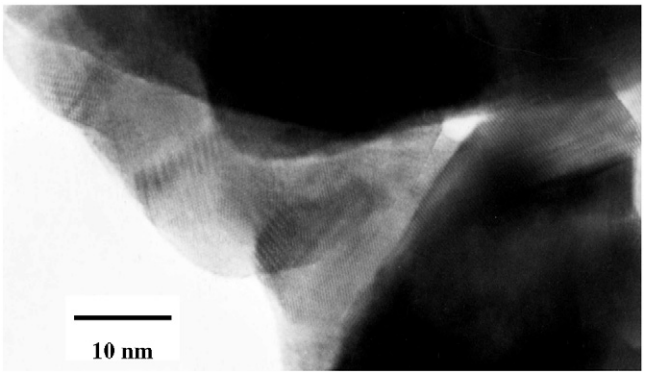

Fig. 4. HRTEM image of sample 6m showing lattice planes of crystallites larger than 10 nm.

3.3. Chemical composition

ICP results of all samples are listed in Table 2. It is obvious that the potassium content is the same in samples F and 70h while it is markedly reduced in sample 6m. This indicates a partial loss of potassium acetate during prolonged use in VAM production which is well known and compensated by re-addition of KOac during time on stream in the technical process. The low K percentage in sample 6m (Table 2) might be due to incomplete re-addition of KOac during reaction. In all samples, a certain amount of K remained after KOac removal. This can be due to limited effectiveness of the removal procedure and/or a more stable bonding of parts of potassium to the catalyst surface, e.g. by inclusion in the support structure.

Due to the variation in the K and C content, the comparison of metal/Si ratios is more meaningful than the comparison of absolute metal concentrations. Evidently, the Au/Si ratio remains nearly constant in all samples, suggesting that there is no loss of gold during use in the catalytic reaction. This is different for palladium. A clear decrease of the Pd/Si ratio is observed for sample 6m which points to leaching of Pd during prolonged time on stream. After 70 h use, this effect is still negligible. As a consequence of Pd leaching, the Pd/Au ratio in sample 6m decreases, too. Moreover, a significant decrease of the Pd/Si and Pd/Au ratio is observed for sample 6m-K. This points to the presence of water-soluble Pd (possibly in form of Pd acetate) which might have formed during prolonged time on stream and is removed by the washing procedure. This is not yet evident after 70 h use. As expected, the carbon content decreases in all samples after the removal of KOac, however, stays surprisingly high in sample 70h-K. An explanation for this observation arises from FTIR studies described below.

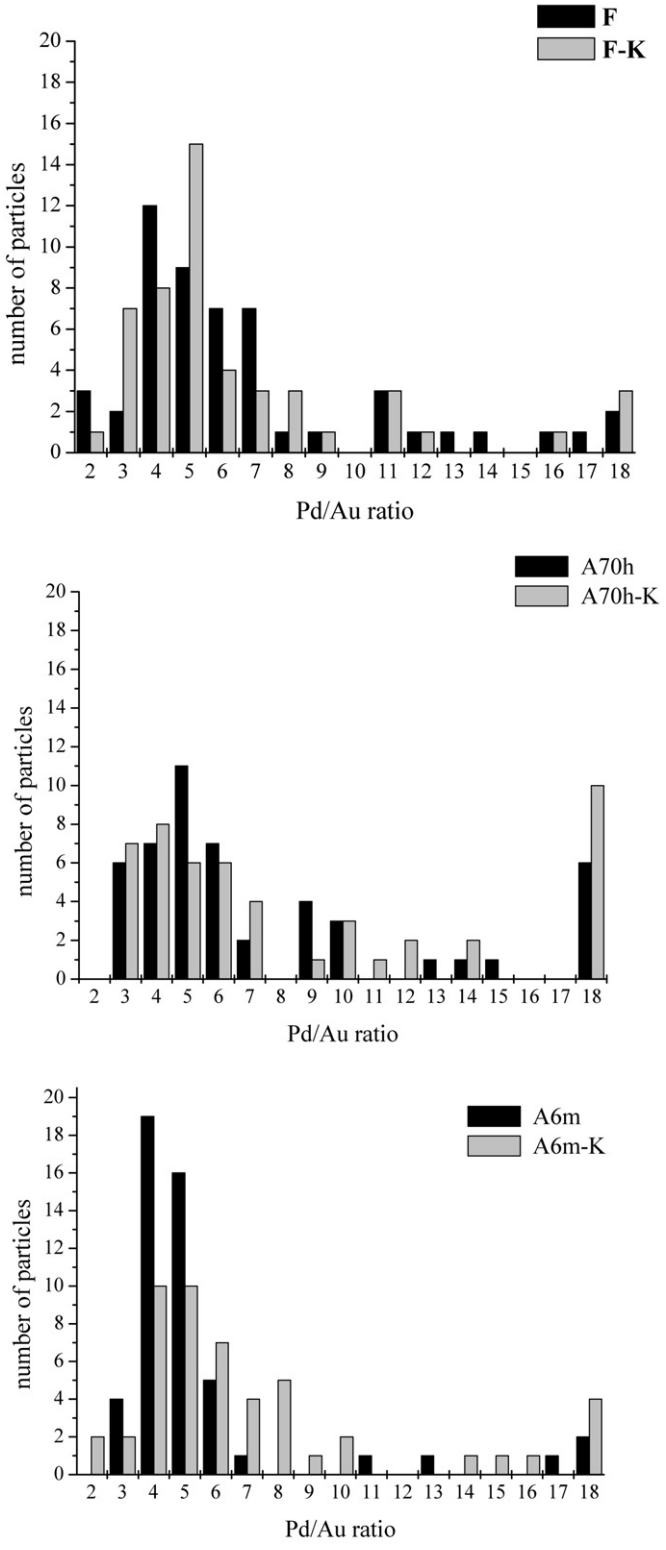

Fig. 5. Distribution of the Pd/Au ratio obtained by EDX measurements of 50 different metal particle areas for as received samples F, 70h and 6m (black columns) as well as after KOac removal (grey columns). Column 18 represents all ratios starting from 18 to pure Pd.

3.4. CO adsorption studied by FTIR

FTIR analysis of adsorbed CO is a well-known tool to analyse the nature of Pd sites exposed on the catalyst surface [14]. Therefore, it is used in this work to characterise Pd sites in samples after KOac removal. Spectra of all samples measured at ambient temperature after pretreatment (1 h evacuation at 200 °C) are plotted in Fig. 6. The band intensities of the Si–OH vibrations around 3640 cm^{-1} decrease with increasing time on stream (Fig. 6a). Simultaneously the broad bands around 3650 cm^{-1} indicating associated OH groups become more intensive which is seen by comparison of the respective band intensities (3740/3650 cm^{-1}). This can be explained by changes of the support surface structure and/or area and by adsorbed water remaining from the KOac remove procedure at low temperatures. In sample 70h-K additional bands arise from carbonyl (1732 cm^{-1}) and CH deformation vibrations (1420 and 1380 cm^{-1}) which, however, cannot be explained by potassium acetate (Fig. 6b). Rather they arise from another strongly adsorbed organic compound at the surface, which could consist of oligomers or low polymers of VAM. Similar deposits were previously found especially at low reaction temperatures (155 °C). They decomposed upon heating by liberating acetic acid [12]. However, it cannot be completely excluded that the band 1732 cm^{-1} is at least partly arising from a monodentate ester-like Pd acetate surface species as observed similarly by Macleod et al. [13]. The fact that this band is not seen anymore in sample 6m-K

Table 2
Results of chemical analysis by ICP-OES.

Sample	K wt%	C wt%	Pd/Au at. ratio	Pd/Si at. ratio × 10^{-3}	Au/Si at. ratio × 10^{-3}
F	2.08	1.65	4.53	9.8	2.2
F-K	0.37	0.14	4.47	9.7	2.2
70h	2.09	1.43	4.54	9.6	2.1
70h-K	0.58	0.49	4.57	9.6	2.1
6m	1.87	1.18	4.23	8.9	2.1
6m-K	0.5	0.2	4.15	8.7	2.1

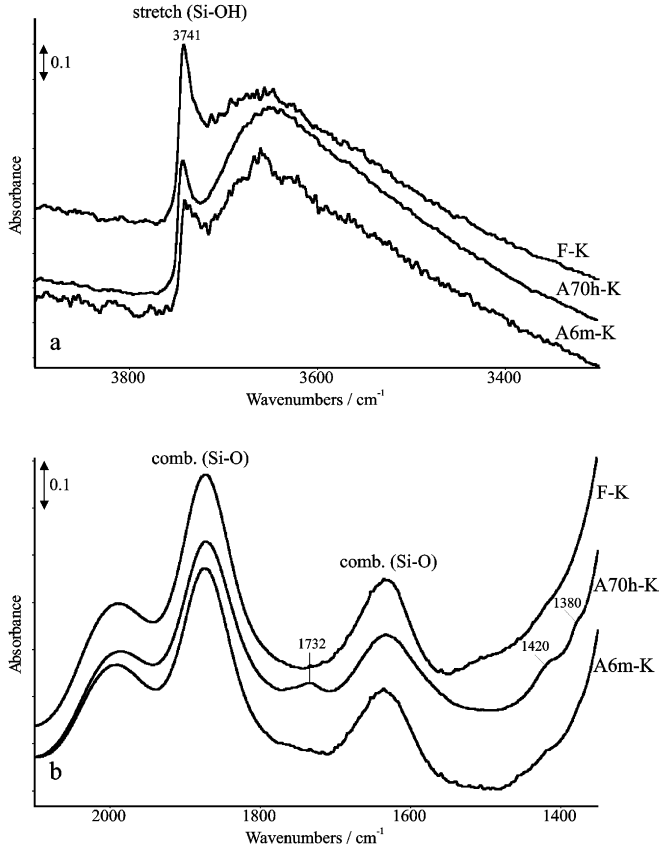

Fig. 6. FTIR spectra of samples F-K, 70h-K and 6m-K measured in different wavenumber ranges at room temperature after 1 h evacuation at 200 °C.

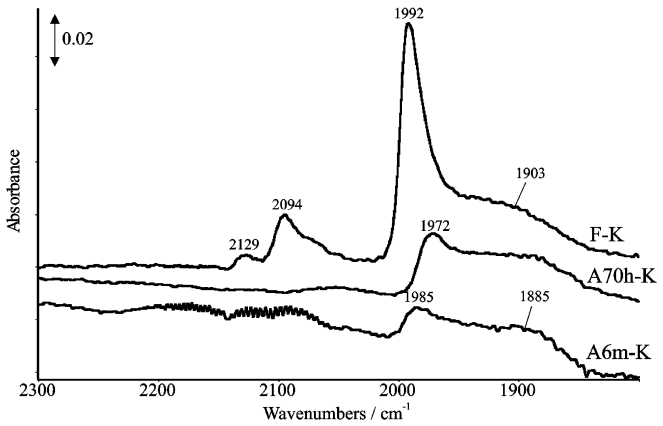

Fig. 7. Background subtracted FTIR spectra of adsorbed CO on samples F-K, 70h-K and 6m-K.

could, besides missing accumulation of organic surface deposits, be connected to the formation of water-soluble Pd acetate which might have been washed out together with KOac. Background-subtracted spectra obtained after adsorption of CO at ambient temperature are presented in Fig. 7. A number of different carbonyl bands are observed. According to literature data [12,14] they are assigned to linear bound Pd^0–CO (2058–2085 cm^{-1}), isolated bridged $(Pd^0)_2$–CO (1925 cm^{-1}), triply bridged $(Pd^0)_3$–CO (1872–1905 cm^{-1}) and compressed bridged $(Pd^0)_2$–CO (1974–1982 cm^{-1}). The latter CO species have to be understood as bridged carbonyl species which are adsorbed closely enough to directly interact with one another, i.e. each Pd centre is bound to two bridging carbonyls.

From Fig. 7 it is evident that all types of CO species are present on the fresh catalyst F while only compressed–bridged and triply bridged CO species can be detected on the surface of the used catalysts 70h and 6m. This suggests that the Pd–Pd distances decrease during deactivation, i.e., the Pd atoms become more closely packed [12]. Thus, less CO molecules are needed to cover the exposed Pd surface area. This can also be one reason for the decrease of the total band intensity, which relates to the number of adsorbed CO molecules. On the other hand, longer distances between neighbouring Pd sites in the fresh catalyst could be due to the fact that Au atoms are located in close contact with Pd atoms, thus, diluting the Pd surface as interpreted in [12]. Then the decrease of the Pd–Pd distances could be due to a diffusion of the diluting Au atoms into the bulk of the metal particle or, vice versa, a diffusion of Pd out of the bulk leading to an enrichment of the surface in Pd. Another reason for the essential decrease of carbonyl band intensities may be the higher amount of associated OH groups found on the aged VAM catalysts in comparison to the fresh sample (*cf.* Fig. 6a). These OH groups can hinder the adsorption of CO by blocking a part of the Pd adsorption sites.

3.5. XPS results

TEM and XRD results indicate that the samples consist of noble metal alloy particles supported on the silica primary particles. However, the above described ICP and TEM results also suggest that there exist mobile Pd species which can be redistributed during time on stream and KOac removal. To include all coexisting kinds of Pd species, XPS measurements have been performed on as-received samples before and after KOac removal as well as on ground samples before and after KOac removal. For all samples next to O 1s and C 1s the Pd 3d, Au 4f, K 2p and Si 2p peaks were collected and evaluated with respect to the binding energy and atomic ratios (Pd/Au, Au/Si and Pd/Si.). The atomic ratios will be discussed in comparison to the ICP results to derive information on bulk/surface composition differences.

XPS spectra of unground samples before and after KOac removal are shown in Fig. 8. In samples F, 70h and 6m the Pd peak intensity is very low while the Au peak intensity is even below the detection limit (Figs. 8a and 8b). The low intensity of the peaks might be due to the inclusion of the noble metal phase beneath the catalyst secondary particle surface, which renders most of the metal phase non-accessible by XPS. A slight increase of the Pd intensity is observed with increasing ageing. Moreover, the Pd 3d peaks are shifted to higher binding energy in sample 6m pointing to partial oxidation (Fig. 8a). This suggests, that after extended time on stream, some soluble Pd (possibly Pd acetate) may form which is able to migrate to the catalyst particle surface. An increase of the Pd peak intensity can be observed after removal of KOac for all unground samples (Fig. 8c). The electron binding energy around 335.0 eV indicates mostly metallic Pd. Only for sample 6m-K a peak at 335.8 eV was found which is typical for oxidised Pd. While the bulk Pd/Si ratio derived by ICP is lowest for sample 6m-K due to leaching of Pd (Table 2), the surface Pd/Si ratio derived by XPS from unground sample 6m-K is highest (Fig. 8c). This supports the assumption that, with extended times on stream, Pd might be dissolved from the metal particles forming a mobile Pd component (probably Pd acetate). Obviously, the washing procedure for KOac removal promotes the migration of this mobile, partially oxidised Pd component to the catalyst surface. Au still remains at the detection limit (Fig. 8d), which means that Au persists below the outermost surface.

For further experiments the samples were ground. This leads to the formation of smaller particles with new surfaces, which were hidden in the bulk before grinding and become now accessible by XPS. Due to the XPS information depth of about 10 nm, the composition observed by XPS should be equal to the bulk composition for particles smaller than 20 nm. For larger particles only the near-surface region of the particles can be probed by XPS. Thus, comparison of unground and ground samples, reflecting preferably the bulk and surface composition, respectively, should tell whether a component is located preferably in the bulk or at the macroscopic surface of the catalyst particles.

As expected, higher metal/Si ratios were found after grinding and Au became detectable for all samples (compare Figs. 8 and 9). In contrast to the results of the unground samples, a general trend to lower Pd/Si values could be observed for the aged samples. This result supports the hypothesis of a migration of Pd from the embedded particles to the surface. Considering the Pd 3d peaks, it is evident that only sample 6m shows hints for oxidised Pd (shoulder at 342.7 eV for the Pd $3d_{3/2}$ in Fig. 9a) while in all other samples Pd is essentially zerovalent. This confirms the weak trend observed already for the unground sample 6m (Fig. 8).

Potassium has been detected in all samples before KOac removal. In sample F before and after grinding, the binding energy of the K $2p_{3/2}$ electrons is 292.7 eV, while in the used samples 70h and 6m a slight binding energy shift of 0.5 eV to higher values is observed. These values are typical for monovalent K. The slight shift points to changes in the neighbourhood of the K ions during time on stream. The K/Si ratio decreases from 0.20 in sample F to 0.16 in sample 6m. Virtually the same values were observed after grinding. This hints to partial incorporation of K into the lattice of SiO_2 which is also supported by the higher K content found by ICP for the aged samples after KOac removal. Besides the net loss of KOac in the used samples which is also evident from ICP data (Table 2), these results indicate the homogeneous distribution of KOac over the catalyst particles.

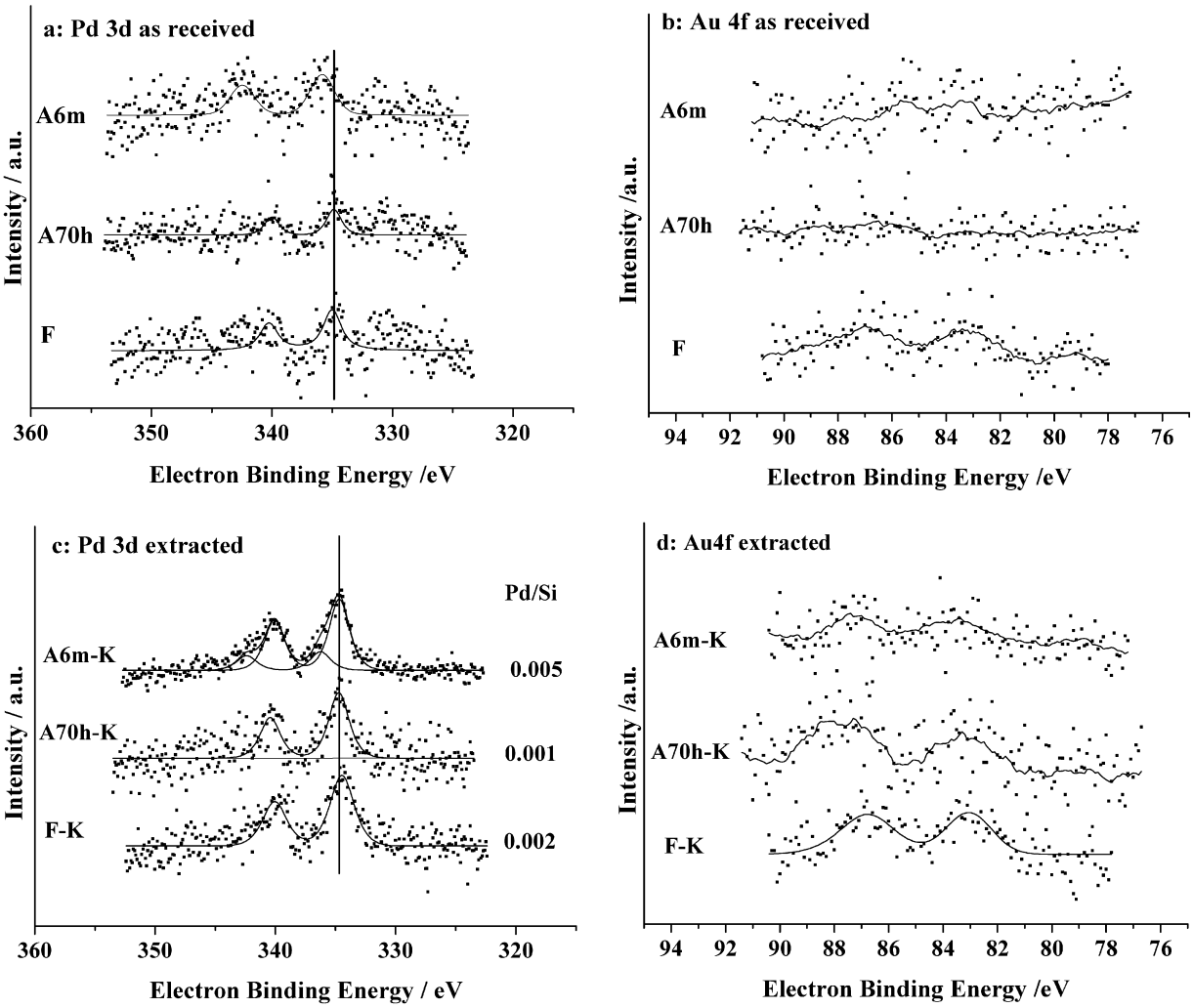

Fig. 8. Normalised Pd 3d (a, c) and Au 4f XP spectra (b, d) of unground samples before (a, b) and after KOac removal (c, d).

4. Discussion

4.1. Structure and composition of metal particles

When comparing XRD and TEM results, some striking discrepancies become obvious which call for a plausible explanation. XRD powder patterns reveal mean crystallite sizes between 3.8 and 5 nm and mean Pd/Au alloy compositions between 1:1 and 0.9:1.1. The latter values are in strong disagreement with the overall Pd/Au ratio amounting to 4.6 and suggest that a considerable part of the total Pd might be XRD-invisible. In contrast to XRD, a broad variety of alloy compositions ranging from Pd/Au = 2 to pure Pd and crystallite sizes with largest values exceeding 10 nm is detected by TEM/EDX in all samples (Figs. 2–5).

To understand this disagreement, the XRD data evaluation procedure must be critically reconsidered. The crystallite size is determined from the peak width using the Scherrer equation. The broader the peak, the smaller the crystallites appear. It is important to note, that this evaluation provides only mean values averaging over all crystallite sizes present in the sample. The fact that crystallites larger then 10 nm exist in the samples, as detected by TEM, means that an unknown number of narrower sub-peaks from larger crystallites is hidden under the experimental XRD peak which reflects only their envelope and, thus, simulates the prevalence of smaller crystallites which does not reflect reality. Deconvolution of the experimental peak into narrower sub-peaks to derive crystallite sizes that agree with TEM results does, however, not make sense since the choice of such sub-peaks would always be voluntary and more than one solution would fit the experimental peak, depending on the number and line width of the considered sub-peaks. Since the alloy composition is derived from the position of the peak maximum, it is also clear that, with the overlay of sub-peaks at different positions, a wide distribution of Pd/Au ratios must exist which, in fact, is in line with the TEM results. Thus, XRD can neither give the real crystallite sizes nor the real distribution of the composition, as long as both properties vary within certain limits throughout the sample. This has not been adequately considered in the previous study on aged VAM catalysts by Macleod et al. [13]. Moreover, it means that it is not appropriate to conclude that a considerable part of the Pd is XRD-invisible. In fact HRTEM, which better reflects reality, shows crystallite agglomerates of rather high Pd percentage (Figs. 2–5). Good conclusion.

Additionally, there is a discrepancy between XRD and TEM with respect to crystallinity. A marked loss of crystallinity (sample 70h) followed by partial recrystallisation upon time on stream (sample 6m) was observed by XRD. In HRTEM micrographs, this should be reflected by a decrease of the crystallite size below ≈3 nm which is the limit for visibility by XRD. However, this is not the case in Fig. 4, in which lattice planes of larger crystallites are properly seen. It has to be taken into account that the total difference between the cubic lattice constants of pure Au (0.4080 nm) and pure Pd (0.3890 nm), forming the outer limits of the completely misci-

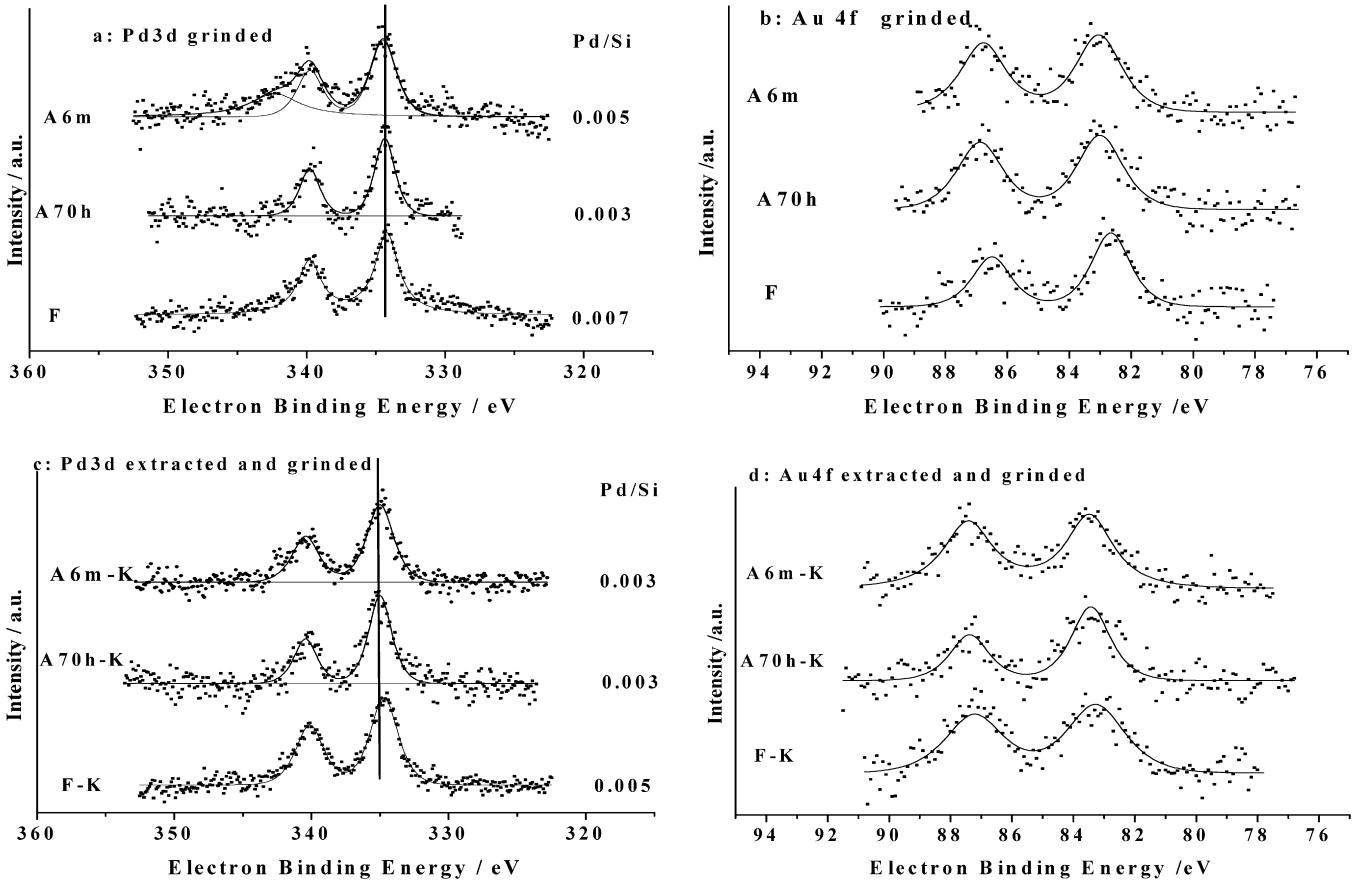

Fig. 9. Normalised Pd 3d (a, c) and Au 4f XP spectra (b, d) of ground samples before (a, b) and after KOac removal (c, d).

ble Pd/Au system, is only 0.02 nm. This means that the distances between subsequent 200 or 111 lattice planes, which are preferably observed in HRTEM (Fig. 4), would differ by only 0.01 nm in the case of pure Pd and Au. For binary compositions within the Pd/Au system this difference would be even smaller than 0.01 nm. TEM cannot detect such small differences in the distances between subsequent lattice planes and, consequently, is also unable to detect changes in the Pd/Au ratio of single crystallites. Thus, for TEM the crystallites would appear unchanged in their size and contrast. Indeed, this has been experimentally observed for single-phase carbon-supported Pd/Au particles in the liquid phase oxidation of glycerol, which showed leaching of palladium connected with variation of the Pd/Au alloy compositions while the crystallite size determined by TEM remained apparently constant [15].

This would be different for XRD which requires a certain long-range order with constant distances between subsequent lattice planes to detect the related reflection peak. The above discussed very small deviations in lattice plane distances arising from changes of the Pd/Au alloy composition within a single TEM-detected crystallite would lead to a loss of long-range order in XRD and, thus, to strong broadening and intensity loss of the XRD reflections. While no XRD data were provided in Ref. [15], this is indeed observed for the used VAM catalysts 70h and 6m studied in the present work and can account for the discrepancies in TEM and XRD results. Moreover, this consideration clearly shows that a reliable interpretation of the results can only be realised by the integrated evaluation of both XRD and TEM experiments, an important issue which has been widely disregarded so far. For prospective investigations of VAM catalysts electron diffraction patterns at high camera length should be taken into account to get information on the distribution of spots within the ring patterns of the 111 and 200 reflections of the Pd/Au alloys. This could provide further insight into the differences between TEM and XRD results.

4.2. Formation of mobile Pd species

The net loss of Pd during time on stream evident from ICP results (samples 6m and 6m-K, Table 2) as well as the narrowing of the compositional distribution at lower Pd/Au ratios especially in the long-time used sample 6m (Fig. 5) point to the formation of mobile Pd species, which are partially leached out during reaction. The leaching step should be preceded by migration of Pd from the metal species to the surface of the catalyst particle. The higher Pd intensity detected by XPS in the unground sample 6m in comparison to samples F and 70h (Fig. 8a) supports this assumption. Moreover, the additional loss of Pd after washing off KOac (sample 6m-K, Table 2) and the redistribution observed by TEM/EDX (sample 6m-K, Fig. 5) clearly show that this mobile Pd is soluble in water. The valence state is probably >0, as indicated by the shift of the Pd binding energy of a shoulder to higher values in samples 6m and 6m-K (Figs. 8 and 9). Based on these results, it is very likely that metallic Pd is partially dissolved to form Pd acetate.

Interestingly, ICP, TEM/EDX and XPS results reveal the most striking change between samples 70h and 6m while the difference in the properties between samples F and 70 is only marginal. In contrast, XRD and FTIR suggests that the most obvious change occurs within the first 70 h on stream (compare sample F-K and 70h-K in Fig. 7 and Table 1). To explain this discrepancy, the information depth of the methods must be considered. While CO chemisorption (FTIR) provides information exclusively from the outermost surface layer of the sample, ICP, XRD and TEM/EDX are true bulk techniques comprising the whole sample volume and

also XPS probes up to about 10 atomic subsurface layers. Thus, the fact that FTIR detects a decrease of the Pd–Pd distances reflecting an enrichment of the metal particle surface in palladium within the first 70 h on stream whereas almost no soluble Pd is evidenced by the other methods in sample 70h and 70h-K suggests, that the process of Pd migration from the metal particle bulk to the surface might take place in the early stage of reaction (70 h) which acts as a activation and stabilisation period for the catalyst. The dissolution as Pd acetate which can be irreversibly removed by washing with water (sample 6m-K) might require longer times (6 months). Catalytic tests revealed that the catalyst looses about 10% of its initial peak activity (measured as space time yield of VAM) during the first 20 h and approaches a pseudo-steady state in which further deactivation does not influence selectivity markedly. The fact that this process obviously goes along with an enrichment of the metal particle surface with Pd agrees very well with observations on model systems by Chen et al. [9]. These authors identified single Pd atoms isolated from each other by surrounding Au atoms as active sites in a catalyst consisting of Pd atoms deposited on Au (100) and Au (111) single crystal surfaces. They observed a dramatic decrease of the activity (TOF values) when the Pd surface concentration exceeded 0.05 monolayers, i.e., with decreasing distance between the Pd atoms on the surface. Regarding the FTIR results in this work, it is probable that, due to the mobility of Pd, the Pd surface concentration in the real catalysts increases during the early stages of reaction. This might be one reason for the above mentioned activity loss during the first 70 h but, on the other hand, leads to stabilisation of the catalyst in a pseudo-steady state, probably due to the establishment of an equilibrium between Pd still fixed on the metal particle surface and Pd dissolved in the liquid KOac/acetic acid/water layer assumed to cover the metal particles [5,13]. Thus, after long time use the FTIR results reveal less change than in the first period.

5. Conclusions

Based on the results obtained by comprehensive characterisation with different techniques and following the ideas outlined in the discussion above, some relations between changes of catalyst properties and loss of catalytic activity can be identified:

In contrast to previous studies, sintering is not an issue for the catalyst studied in this work up to 6 month use, although a marked loss of activity was observed.

Despite the fact that no sintering occurs, the metal particles undergo dynamic restructuring connected with a dramatic loss in XRD-sensitive crystallinity during the first 70 h on stream followed by partial recrystallisation during longer use. The fact that this is not adequately reflected by TEM suggests that the crystallites remain epitactically ordered while just the Pd/Au ratio changes in certain areas due to the migration of Pd. This process goes along with an enrichment of the metal particle surface in Pd during the early stages on stream followed by formation of water-soluble Pd, most probably in the form of acetate. Considering earlier studies which identified single Pd atoms isolated from each other by surrounding Au atoms [9], it is probable that the enrichment of Pd on the exposed catalyst surface is a major reason for loss of activity in the present type of catalyst.

Finally it must be mentioned, that the usual XRD procedure [13] for the simultaneous calculation of crystallite sizes and alloy compositions from the width and position of the XRD reflections is not meaningful in such an inhomogeneous system as represented by Pd,Au/SiO_2 catalysts. Instead, a combination of XRD and TEM/EDX investigations is recommended to derive reliable results on metal crystallite size and composition.

Acknowledgments

The authors thank BP Chemicals Ltd and Yorkshire Forward for financial support, and helpful discussions.

References

[1] G. Ertl, H. Knözinger, J. Weitkamp (Eds.), Handbook of Heterogeneous Catalysis, vol. 5, Wiley–VCH, Weinheim, 1997, p. 2295.
[2] S. Nakamura, T. Yasui, J. Catal. 17 (1970) 366.
[3] S. Nakamura, T. Yasui, J. Catal. 23 (1971) 315.
[4] B. Samanos, P. Boutry, R. Montarnal, J. Catal. 23 (1971) 19.
[5] E.A. Crathorne, D. MacGowan, S.R. Morris, A.P. Rawlinson, J. Catal. 149 (1994) 254.
[6] W.D. Provine, P.L. Mills, J.J. Lerou, Stud. Surf. Sci. Catal. 101 (1996) 191.
[7] Y.-F. Han, D. Kumar, C. Sivadinarayana, A. Clearfield, D.W. Goodman, Catal. Lett. 94 (2004) 131.
[8] M. Chen, K. Luo, T. Wei, D. Kumar, C.-W. Yi, D.W. Goodman, Catal. Today 117 (2006) 37.
[9] M. Chen, D. Kumar, C.-W. Yi, D.W. Goodman, Science 310 (2005) 291.
[10] A. Rabl, A. Renken, Chem. Ing. Tech. 5 (1986) 434.
[11] R. Abel, G. Prauser, H. Tiltscher, Chem. Eng. Technol. 17 (1994) 112.
[12] Q. Smejkal, D. Linke, U. Bentrup, M.-M. Pohl, H. Berndt, M. Baerns, A. Brückner, Appl. Catal. A Gen. 268 (2004) 67.
[13] N.M. Macleod, J.M. Keel, R.M. Lambert, Appl. Catal. A Gen. 261 (2004) 37.
[14] W. Daniell, H. Landes, N.E. Fouad, H. Knözinger, J. Mol. Catal. A Chem. 178 (2002) 211.
[15] L. Prati, A. Villa, F. Porta, D. Wang, D. Su, Catal. Today 122 (2007) 386.